Climate Data Record (CDR) Program

Climate Algorithm Theoretical Basis Document (C-ATBD)

VIIRS Land Bundle - Surface Reflectance and Normalized Difference Vegetation Index

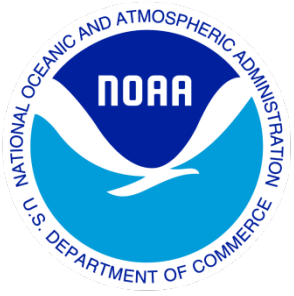

CDR Program Document Number: CDRP-ATBD-1267
Configuration Item Number: 01B-20a & 01B-20b
Revision 0 / April 05, 2022

REVISION HISTORY

Rev.	Author	DSR No.	Description	Date
1	Eric Vermote, NASA and Jose Luis Villaescusa, UMD/NASA	DSR-1605	Initial Submission to CDR Program	12/10/2021

TABLE of CONTENTS

LIST of FIGURES

LIST of TABLES

1. Introduction

1.1 Purpose

The purpose of this document is to describe the algorithm submitted to the National Centers for Environmental Information (NCEI) by Dr. Eric Vermote, NASA/GSFC, Terrestrial Information Systems Branch, Code 619, that will be used to create the VIIRS Surface Reflectance and Normalized Difference Vegetation Index Climate Data Record (CDR), using the Visible/Infrared Imager/Radiometer Suite (VIIRS) sensors onboard the NPOESS Preparatory Project (NPP) spacecraft launched by the National Aeronautics and Space Administration (NASA) and the Joint Polar Satellite System (JPSS) launched jointly by the National Oceanic and Atmospheric Administration (NOAA) and NASA. The actual algorithm is defined by the computer program (code) that accompanies this document, and thus the intent here is to provide a guide to understanding that algorithm, from both a scientific perspective and in order to assist a software engineer or end-user performing an evaluation of the code.

1.2 Definitions

Variable definitions are included as they are described in Section 3.4: Theoretical Description.

1.3 Referencing this Document

This document should be referenced as follows:

VIIRS Surface Reflectance and Normalized Difference Vegetation Index - Climate Algorithm Theoretical Basis Document, NOAA Climate Data Record Program CDRP-ATBD-1267 Rev. 0 (2022). Available at https://www.ncei.noaa.gov/products/climate-data-records

1.4 Document Maintenance

Periodic updates to the algorithm and dataset are possible to occur. This could be (for example) when improvements to the algorithm are developed. Any update will be given a new version number, and an updated version of the C-ATBD will be generated.

2. Observing Systems Overview

2.1 Products Generated

The objective of this algorithm is to retrieve the Bidirectional reflectance distribution function (BRDF)-corrected Surface Reflectance and the associated Normalized Difference Vegetation Index (NDVI) from VIIRS sensors. Additional quality information is provided such as cloud state, cloud-shadow flags, and overall aerosol quality flags. The final products are mapped into daily 0.05°x0.05° grid, corresponding to a 3600x7200 array over the globe.

The following surface reflectance products are generated: a global CMG-grid daily L3 surface reflectance (NPP09C1, JP109C1), and a global CMG-grid daily L3 NDVI product (NPP13C1, JP113C1). See Table 1.

Table 1: Land surface reflectance products included in these CDRs.

Products	NASA Product Type Identifier	Description
Surface Reflectance (L3 Daily CMG products)	NPP09C1 JP109C1	VIIRS Daily Surface Reflectance L3 Global CDR 0.05°x0.05° grid CMG Bands I1-I3, M12, M15, M16. Output is in netcdf format.
NDVI (L3 Daily CMG Products)	NPP13C1 JP113C1	VIIRS Daily NDVI L3 Global CDR 0.05°x0.05° grid CMG Output is in netcdf format.

2.2 Instrument Characteristics

The VIIRS instrument observes and collects global satellite observations that span the visible and infrared wavelengths across land, ocean, and atmosphere. A whiskbroom radiometer by design, it has 22 channels ranging from 0.41 μm to 12.01 μm. Five of these channels are high-resolution image bands or I-bands, and sixteen serve as moderate-resolution bands or M-bands. VIIRS also hosts a unique panchromatic Day/Night band (DNB), which is ultra-sensitive in low-light conditions that allows us to observe nighttime lights with better spatial and temporal resolutions compared to previously provided nighttime lights data by the Defense Meteorological Satellite Program. Details about these bands are shown in Table 2.

Table 2: VIIRS instrument channel summary.

Band Use	Band Name	Center (microns)	Width (Full Width at Half Maximum)
Ocean Color Aerosol	M1	0.415	0.02
	M2	0.445	0.02
	M3	0.49	0.02
	M4	0.555	0.02
Imagery band	I1	0.64	0.075
Ocean Color Aerosol	M5	0.673	0.021
Day/Night Band	DNB	0.7	0.4
Atmospheric Correction	M6	0.746	0.021
NDVI	I2	0.865	0.039
Ocean Color Aerosol	M7	0.865	0.039
Cloud Particle Size	M8	1.24	0.02
Cirrus Cloud Cover	M9	1.378	0.02
Binary Snow Map	I3	1.61	0.06
Snow Fraction	M10	1.61	0.06
Clouds	M11	2.25	0.05
Imagery band Clouds	I4	3.74	0.38
Sea Surface Temperature	M12	3.7	0.18
Sea Surface Temperature/Fires	M13	4.05	0.155
Cloud Top Properties	M14	8.55	0.3
Sea Surface Temperature	M15	10.763	1
Imagery band Clouds	I5	11.45	1.9
Sea Surface Temperature	M16	12.013	0.95

VIIRS is one of five instruments onboard the Suomi National Polar-orbiting Partnership (SNPP) satellite platform that was launched on October 28, 2011. SNPP (formerly called the National Polar-orbiting Operational Environmental Satellite System (NPOESS) Preparatory Project) serves as a bridge between the Earth Observing System (EOS) satellites and the next-generation NASA-NOAA Joint Polar Satellite System (JPSS). Four JPSS missions have been planned to last through 2031, and each of them will host a VIIRS instrument as part of their payload. JPSS-1 (NOAA-20) was launched on November 18, 2017, and JPSS-2 is scheduled to launch in 2022.

The VIIRS sensor was designed to extend and improve upon the series of measurements initiated by its predecessors, the Advanced Very High Resolution Radiometer (AVHRR), the Moderate Resolution Imaging Spectroradiometer (MODIS), and the Sea-viewing Wide Field-of-view Sensor (SeaWIFS). VIIRS-derived data products are used to measure cloud and aerosol properties, ocean color, ocean and land surface temperature, ice movement and temperature, fires, and Earth's albedo. Climatologists use VIIRS data to improve our understanding of global climate change. Technical specifications of the sensor are shown in Table 3.

Table 3: Technical specifications of the VIIRS sensor

Orbit:	830km, 1:30pm mean local solar time. sun-synchronous, polar
Repeat Cycle:	16 days
Swath Dimensions:	3000km, nearly global coverage every day
Weight:	275kg
Spatial Resolution:	750m
Data Rate:	5.9 Mbps
Quantization:	12 bits
Field of View:	deg
Wavebands:	9 visible/NIR bands plus day/night pan band 8 mid-IR 4 LW IR
Design Life:	7 years
Duration:	Operational

3. Algorithm Description

3.1 Algorithm Overview

This is the complete description of the algorithm at the current level of maturity (which will be updated with each revision). The Surface Reflectance algorithm is designed to contain four main subroutines: Extract inputs, Quality Flags, Surface Reflectance Retrieval and Write Surface Reflectance. The Surface Reflectance Retrieval subroutine is the main subroutine since it performs the Lambertian approximation (atmospheric correction), and the bidirectional reflectance distribution function (BRDF) coupling adjustment.

3.2 Processing Outline

The processing outline of the VIIRS Surface Reflectance data processing is summarized in the Data Flow Diagram of Figure 1.

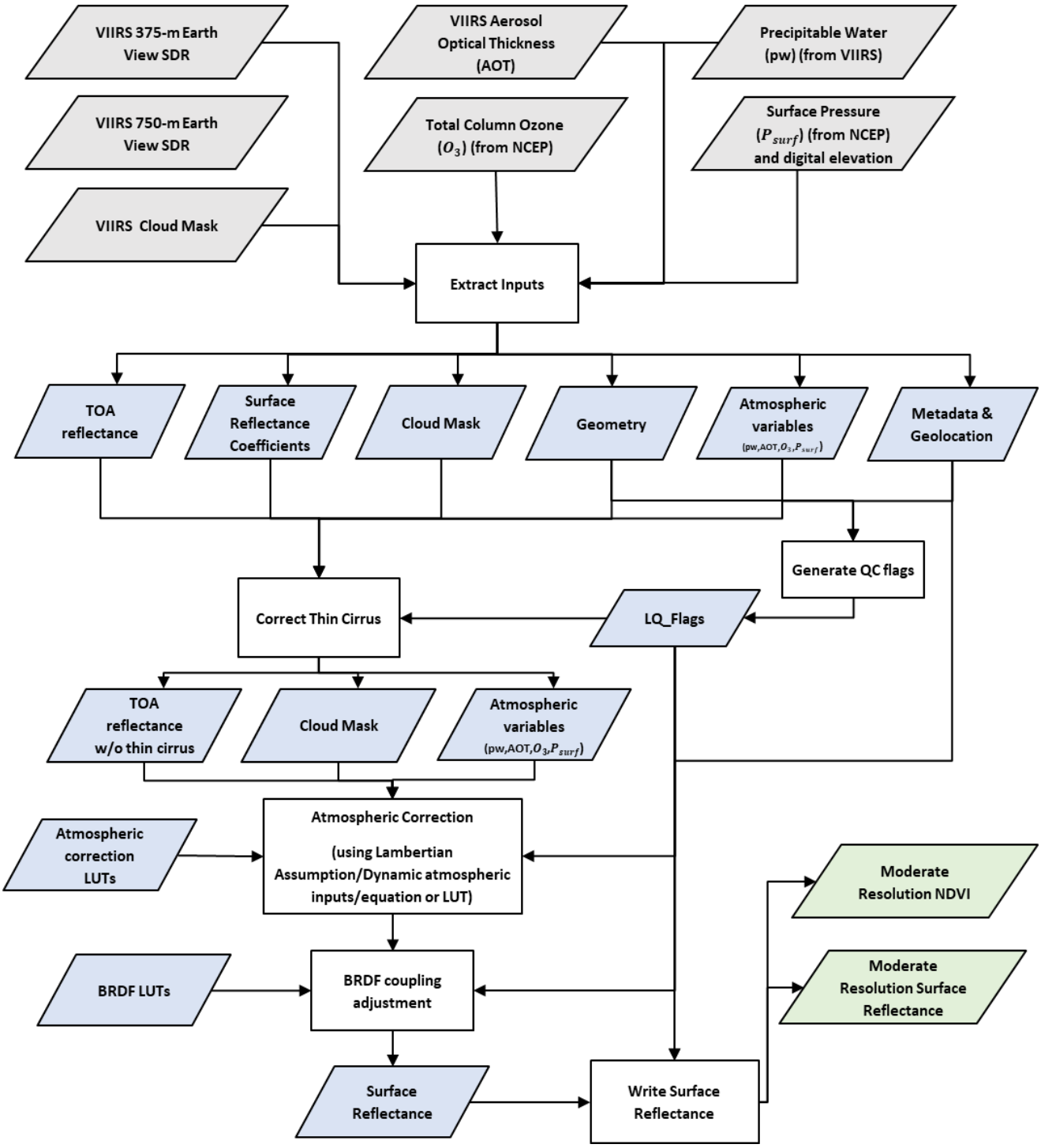

Figure 1: Surface Reflectance processing architecture. Gray represents original inputs, blue the generated outputs, and green the final outputs of the algorithm.

The Surface Reflectance Retrieval routine corrects for the effects of gaseous absorption, molecular and aerosol scattering, thin cirrus contamination, and the coupling of the atmosphere and the surface bidirectional reflectance as a function of the viewing and solar geometries, elevation of the target and spectral band. The atmospheric adjustment

(within the 'Surface Reflectance Retrieval' routine) includes updating the correction coefficients with 'in-view' total column water vapor, ozone, and aerosol optical thickness data input fields. The aerosol information required for surface reflectance retrieval comes from the VIIRS Aerosol Optical Thickness (AOT) and the Aerosol Model Information, complemented by total column water vapor, total column ozone, and surface pressure from National Centers for Environmental Prediction (NCEP) feeds. Backups for these inputs include total column ozone from the Ozone Mapping Profiling Suite (OMPS). The atmospherically corrected surface reflectance values derived using the Lambertian approximation are subsequently adjusted for bi-directional reflectance distribution function (BRDF) effects. The BRDF-coupling adjustment is presently designed after the MODIS approach with a slight modification making the isotropic shape parameter a function of the normalized difference vegetation index, NDVI, (Vermote, 2003), an approximation due to operational constraints and the developmental maturity of the MODIS BRDF-coupling adjustment routine. The surface reflectance values after each adjustment are included as data layers in the surface reflectance along with the Land Quality Flags. The atmospheric inputs are available elsewhere, and the solar and viewing geometries are kept as part of the CDR.

Thin cirrus effects are removed by implementing an empirically based correction using VIIRS band M9 (1.38 μm). The quality control (QC) flags, and the cloud and aerosol quality flag inputs are fused into a single Land Quality Flag (LQF) structure that applies to the Surface Reflectance. The LQF output is appended to the Surface Reflectance. Then the heart of the surface reflectance retrieval process begins, by converting the cirrus effects adjusted satellite reflectance values into surface reflectance values assuming the surface is Lambertian. The earth's surface is generally not Lambertian, and as a result a further correction is applied. The conversion of the at-satellite-reflectance values to surface reflectance requires (i) the use of a set of conversion equations that also account for first order atmospheric multiple scattering effects, and (ii) inputs from pre-generated look up tables (LUTs) and analytic equations for gaseous or molecular effects.

3.3 Algorithm Input

3.3.1 Primary Sensor Data

The Surface Reflectance algorithm uses the following VIIRS data:

- VIIRS Aerosol Optical Thickness
- VIIRS Precipitable Water (fallback water vapor source if it becomes available over land)
- VIIRS 375-m Earth View SDR (including radiances, geometry, geolocation, and elevation for bands I1, I2, I3 and I4)
- VIIRS 750-m Earth View SDR (including radiances, geometry, geolocation, and elevation for bands M1, M2, M3, M4, M5, M7, M8, M10, and M11). The VIIRS M9 band is used for the cirrus correction.
- VIIRS Cloud Mask (including cloud and land/water mask)

3.3.2 Ancillary Data

The Surface Reflectance algorithm uses non-VIIRS data obtained from the National Center for Environmental Prediction (NCEP), the Navy Operational Global Atmospheric Prediction System (NOGAPS), the USGS EROS Archive (GTOPO30) or the Ozone Mapping and Profiler Suite (OMPS) sensor. Details are shown in Table 4.

Table 4: Ancillary data used in this product

Variable	Source	Spatial Resolution	Temporal Resolution
Surface Pressure	NCEP or NOGAPS	0.5°, 1.0°,2.5°	Six-hourly
DEM	USGS GTOPO30	0.01°	-
Precipitable Water	NCEP or NOGAPS	0.5°, 1.0°,2.5°	Six-hourly
Column Ozone	NCEP or NOGAPS or OMPS	0.5°, 1.0°,2.5°	Six-hourly

3.3.3 Derived Data

<Not Applicable>

3.3.4 Forward Models

<Not Applicable>

3.4 Theoretical Description

The retrieval of surface reflectance from electro-optical spectral sensors usually requires calibrating the sensor input to reflectance units and removing the relatively small contribution due to the atmosphere. The principal atmospheric components affecting the top-of-atmosphere (TOA), or at-satellite-reflectance in the range of 0.4-2.5 μm, are shown in Figure 2.

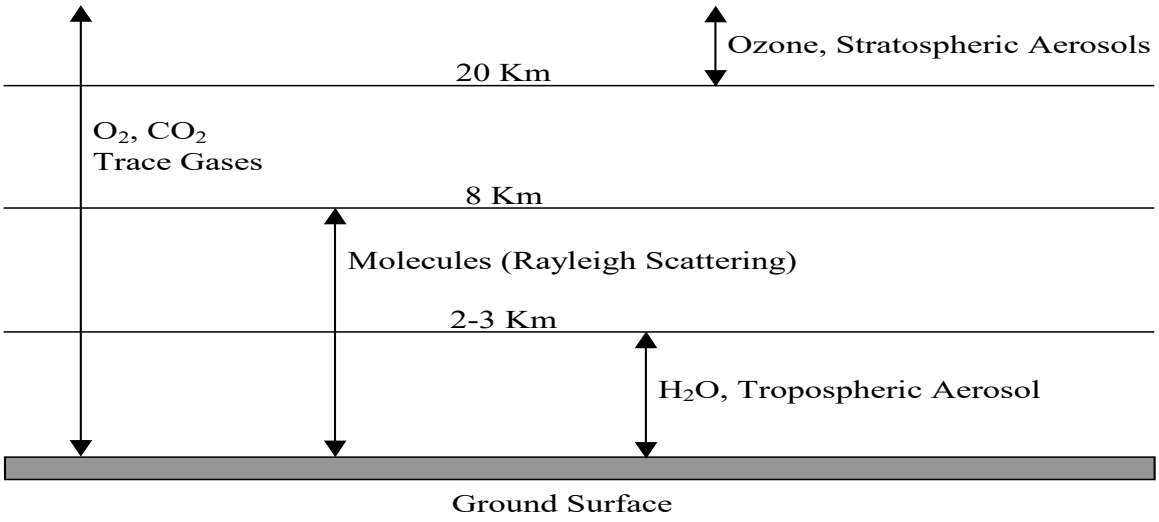

Figure 2: The atmospheric components affecting the remote sensing signal in the 0.4-2.5 μm range.

3.4.1 Physical and Mathematical Description

3.4.1.1 Atmospheric correction

Using the formalism developed for the 6S code, the solution of the radiation transfer equation employing the Lambertian Uniform Target assumption for observation in electro-optical spectral band i, assuming a standard atmospheric profile, but variable ozone and water vapor amount, is written as (Vermote et al.,1997):

$$\begin{aligned}\rho^i_{TOA}(\theta_s,\theta_v,\phi,P,Aer^i,U_{H20},U_{O_3}) \\ = Tg^i_{OG}(m,P)Tg^i_{O_3}(m,U_{O_3})[\rho^i_{atm}(\theta_s,\theta_v,\phi,P,Aer^i,U_{H_20}) \\ + \frac{Tr^i_{atm}(\theta_s,\theta_v,P,Aer^i)\rho_s}{1-S^i_{atm}(P,Aer^i)\rho_s} Tg^i_{H_20}(m,U_{H_20})\ ]\end{aligned} \quad (1)$$

where (dropping the spectral dependence i)

- $Aer^i = (\tau^i_A, w^i_0, P^i_A)$,
- ρ_{TOA} is the reflectance at the top of the atmosphere,
- Tg is the gaseous transmittance by water vapor, Tg_{H2O}, by ozone, Tg_{O3}, or other gases, Tg_{OG} (e.g., CO_2, O_2, CH_4)

- Aer refers to the aerosol model optical properties,
- ρ_{atm} is the atmosphere intrinsic reflectance,
- Tr_{atm} is the total atmosphere transmission (downward and upward)
- $S_{atm}$is the atmosphere spherical albedo,
- ρ_S is the surface reflectance to be retrieved by the atmospheric correction procedure,
- The geometrical conditions are given by θ_s, the solar zenith angle, θ_v, the view zenith angle and ϕ, the difference between the solar and view azimuth angle,
- P is the pressure in Millibars, which influences the number of molecules in the atmosphere and the concentration of absorbing gases,
- (τ_A, w_0, P_A), describe the aerosol properties in band i.
- τ_A is the spectral aerosol optical thickness,
- ω_0 is the spectral aerosol single scattering albedo, describing the absorption of the aerosol, ω_0 is equal to 1 for non-absorption particles, and to 0 for completely absorbing aerosol,
- P_A is the spectral aerosol phase function,
- $U_{H_20}$is the integrated water vapor content in centimeters
- U_{O3} is the integrated columnar ozone content in cm-atm
- m is the air-mass, computed as $m = \frac{1}{\cos(\theta_s)} + \frac{1}{\cos(\theta_v)}$.

The water vapor effect on the atmosphere intrinsic reflectance is approximated in 6S as:

$$\begin{aligned}\rho^i_{atm}(\theta_s, \theta_v, \phi, P, Aer^i, U_{H20}) \\ &= \rho^i_R(\theta_s, \theta_v, \phi, P) \\ &+ \left(\rho^i_{R+Aer}(\theta_s, \theta_v, \phi, P, Aer^i) - \rho^i_R(\theta_s, \theta_v, \phi, P)\right) Tg^i_{H20}\left(m, \frac{U_{H_20}}{2}\right)\end{aligned} \quad (2)$$

where $\rho_R$represents the atmospheric reflectance due to molecular (Rayleigh) scattering, and ρ_{R+Aer} represents the reflectance of the combined molecular and aerosol components, which is computed in 6S using the successive order of scattering method, and thereby accounting correctly for the so-called coupling effect (Deschamps et al., 1983). This approximation conserves the correct computation of the coupling and supposes that the water vapor is mixed with aerosol and that the molecular scattering is not affected by the water vapor absorption. This approximation is reasonable in most cases where observation bands are narrow and outside the water vapor strong absorption, as is the case for VIIRS or MODIS.

The total atmosphere transmission, T_r, is further decomposed into downward and upward terms, which are respectively dependent on θ_s and θ_v and are computed using the same function by virtue of the reciprocity principle, that is:

$$Tr^i_{atm}(\theta_s, \theta_v, P, Aer^i) = T^i_{atm}(\theta_s, P, Aer^i)T^i_{atm}(\theta_v, P, Aer^i) \quad (3)$$

3.4.1.2 Lambertian infinite target correction implementation and operational approach

In the implementation of the algorithm, functions related to atmospheric scattering and absorption, ρ_{atm}, T_{atm} and S_{Atm} are interpolated from pre-computed look up table since they cannot be simply modeled. On the other hand, the gaseous transmission functions can be written as simple analytical expressions. The molecular reflectance term can be computed very efficiently using a semi-empirical approach based on the decomposition suggested by Chandrasekhar. Using the approximation given below in (4), the dependence on the atmospheric pressure can be accounted for, by only computing ρ_{R+Aer} at standard pressure, P_0, which substantially reduces the dimension of the look-up tables. We use:

$$\begin{aligned}\rho^i_{atm}(\theta_s, \theta_v, \phi, P, Aer^i, U_{H20}) &= \rho^i_R(\theta_s, \theta_v, \phi, P) \\ &+ \left(\rho^i_{R+Aer}(\theta_s, \theta_v, \phi, P_0, Aer^i) - \rho^i_R(\theta_s, \theta_v, \phi, P_0)\right) Tg^i_{H20}\left(m, \frac{U_{H_20}}{2}\right)\end{aligned} \quad (4)$$

A similar approach is applied to the atmospheric transmission term, that is:

$$T^i_{atm}(\theta, P, Aer^i) = T^i_{atm}(\theta, P_0, Aer^i)\frac{T^i_R(\theta, P)}{T^i_R(\theta, P_0)} \quad (5)$$

Where T_R is the atmosphere transmission function due to molecular components and θ represents either θ_s or θ_v.

The code implements Equations (1) through (5), using a look-up table approach and analytic expressions. The following section details the computation of each term in the computer code.

3.4.1.2.1 Gaseous transmission

The gaseous transmission by gases, other than water vapor or ozone,$Tg^i_{OG}(m, P)$, in the VIIRS bands can written as a function of the air mass, m, and the pressure P (in atm), as follows:

$$\begin{aligned}Tg^i_{OG}(m, P) = \exp\Big[&m\left(a^i_0 P + a^i_1 \,\mathrm{Log}(P)\right) + \mathrm{Log}(m)\left(b^i_0 + b^i_i Log(P)\right) \\ &+ mlog(m)\left(c^i_0 + c^i_1 Log(P)\right)\Big]\end{aligned} \quad (6)$$

The coefficients $(a^i_0, a^i_1, b^i_0, b^i_1, c^i_0, c^i_1)$ are determined by curve fitting.

The ozone gaseous transmission, $Tg^i_{O_3}(m, U_{O_3})$, in the narrow VIIRS bands (i.e., in the Chappuis band) could be simply modeled as:

$$Tg^i_{O_3}(m, U_{O_3}) = e^{-ma^i_{O_3}U_{O_3}} \quad (7)$$

The coefficients $a^i_{O_3}$ are determined by curve fitting. The units of U_{O_3} are cm-atm.

The water vapor transmission, $Tg^i_{H_2O}(m, U_{H_2O})$, is modeled as:

$$Tg^i_{H_2O}(m, U_{H_2O}) = \exp\left[a^i_{H_2O} mU_{H_2O} + b^i_{H_2O} Log(mU_{H_2O}) + c^i_{H_2O} mU_{H_2O} Log(mU_{H_2O})\right] \quad (8)$$

The coefficients $(a^i_{H_2O}, b^i_{H_2O}, c^i_{H_2O})$ are determined by curve fitting.

3.4.1.2.2 Molecular atmospheric reflectance at standard and actual pressure

The molecular atmospheric reflectance at standard pressure, $\rho^i_R(\theta_s, \theta_v, \phi, P_0)$, is computed by the subroutine CHAND.f, which takes as input, the geometry (μ_s, μ_v, ϕ), where μ_s (resp. μ_v) is the cosine of the solar (resp. view) zenith angle, and ϕ the relative azimuth and the molecular optical thickness in that case at standard pressure, which is pre-computed by 6S, τ_R.

The molecular atmospheric reflectance at actual pressure adjustment, $\rho^i_R(\theta_s, \theta_v, \phi, P_0)$, is simply done by adjusting the amount of molecule or the molecular optical thickness, according to:

$$\tau_R(P) = P\tau_R \quad (9)$$

where the pressure P is expressed in atmospheres.

3.4.1.2.3 Intrinsic reflectance at standard pressure

The intrinsic atmospheric reflectance at standard pressure, $\rho^i_{R+Aer}(\theta_s, \theta_v, \phi, P_0, Aer^i)$, is pre-computed by 6S in a look table for each band and each aerosol model (P_A, ω_0, τ_A). The step in solar zenith angle is 4 deg, in view angle is 4 deg corresponding to the gauss quadrature of 24 angles (with the nadir added), the step is kept constant in scattering angle (4 degree), Θ, which is defined as:

$$\cos(\Theta) = -\cos(\theta_s)\cos(\theta_v) - \cos(\phi)\sin(\theta_s)\sin(\theta_v) \quad (10)$$

resulting in a variable number of steps for each θ_s, θ_v configuration. The indexing to the correct values in the lookup table is achieved using the ANGLE lookup table, which keeps track of the number of geometries computed for each θ_s, θ_v configuration. While more expensive, and more complicated to interpolate within, this structure achieves a higher precision with a reduced size look up table, for a term whose accuracy is critical to the atmospheric correction.

The step in aerosol optical depth is variable to optimize the performance of the correction with the error induced by the interpolation (i.e. finer a low optical depth).

3.4.1.2.4 Atmospheric transmission at standard pressure

Atmospheric transmission, $T_{atm}^{i}(\theta, P, Aer^{i})$, is pre-computed using 6S, with the successive order of scattering method assuming the bottom of the layer is illuminated with isotropic light. The code accounts for the mixing of aerosol molecules within the atmosphere. The values are computed with a step of 4° in θ and for each aerosol model and each band for the predefined values of τ_A. The interpolation for any θ and τ is relatively straightforward since this table has only 2 dimensions. The table volume is also very modest.

3.4.1.2.5 Molecular (Rayleigh) transmission at standard pressure and actual pressure

The molecular transmission, $T_R^i(\theta, P_0)$, at standard pressure is computed using the value of molecular optical depth at standard pressure, τ_R. Using the two-stream method, the molecular transmission is approximated by:

$$T_R^i(\theta, P_0) = \frac{\left|\frac{2}{3}+\cos(\theta)\right|+\left|\frac{2}{3}-\cos(\theta)\right| e^{-\frac{\tau_R}{\cos(\theta)}}}{\frac{4}{3}+\tau_R} \tag{11}$$

The Rayleigh transmission at actual pressure, $T_R^i(\theta, P)$, determination uses the same method, we simply replace τ_R with $\tau_R(P)$ of Equation (9).

3.4.1.2.6 Atmosphere spherical albedo at actual pressure

The atmospheric spherical albedo at actual pressure, $S_{atm}^{i}(P, Aer^{i})$, is defined as:

$$S_{atm}^{i}(P, Aer^{i}) = \int_0^{\frac{\pi}{2}} \int_0^{\frac{\pi}{2}} \int_0^{2\pi} \rho_{atm}^{i}(\theta_s, \theta_v, \phi, P, Aer^{i}) \sin(\theta_s) \cos(\theta_v)\, d\theta_s d\theta_v d\phi \tag{12}$$

By ignoring the water vapor dependence on the atmosphere intrinsic reflectance (S acting as a second order effect), we can write the same relation we have written for the atmosphere intrinsic reflectance, that is

$$S_{atm}^{i}(P, Aer^{i}) = \left(S_{atm}^{i}(P_0, Aer^{i}) - S_R^i(P_0)\right) + S_R^i(P) \tag{13}$$

The $S_{atm}^{i}(P_0, Aer^{i})$ is stored in a pre-calculated look up table depending only on aerosol optical depth and model. The $S_R^i(P)$ term is computed by an analytic expression based on the integral of Equation (12) that is

$$S_R^i(P) = \sum_j a_j EXPI(\tau_R, n) \tag{14}$$

where EXPI is the exponential integral function (see 6S code for details; Vermote et al., 1994).

3.4.1.3 BRDF atmosphere coupling correction

If the target is of infinite dimension, under the Lambertian assumption, the equation of transfer (here rewritten without gaseous absorption to simplify the writing and dropping the spectral dependence) is:

$$\rho_{TOA} = \rho_{R+Aer} + \frac{T_{R+Aer}(\theta_s)T_{R+Aer}(\theta_v)\rho_s}{1 - S_{R+Aer}\rho_s} \tag{15}$$

If we account for the fact that it is not a Lambertian reflector, it can be written as (Vermote et al., 1997)

$$\begin{aligned}\rho_{TOA}(\mu_s, \mu_v, \phi) &= \rho_{R+Aer}(\mu_s, \mu_v, \phi) + e^{-\tau/\mu_s}e^{-\tau/\mu_v}\rho_s(\mu_s, \mu_v, \phi) + e^{-\frac{\tau}{\mu_v}}t_d(\mu_s)\overline{\rho_s} \\ &+ e^{-\frac{\tau}{\mu_s}}t_d(\mu_v)\overline{\rho_s}' + t_d(\mu_v)t_d(\mu_s)\overline{\overline{\rho_s}} + \frac{T_{R+Aer}\mu_s T_{R+Aer}S_{R+Aer}\,(\overline{\overline{\rho_s}})^2}{1 - S_{R+Aer}\overline{\overline{\rho_s}}}\end{aligned} \tag{16a}$$

with $\overline{\rho_s}$, $\overline{\rho}'_s$, and $\overline{\overline{\rho_s}}$ being the terms accounting for the coupling between the atmosphere and the surface BRDF, if the target is Lambertian then $\overline{\rho_s} = \overline{\rho}'_s = \overline{\overline{\rho_s}} = \rho_s$; otherwise, we have:

$$\overline{\rho_s}'(\mu_s, \mu_v, \phi) = \frac{\int_0^{2\pi}\int_0^1 \mu L^{\downarrow}_{R+A}(\mu_s, \mu, \phi')\phi_s(\mu, \mu_v, \phi' - \phi)d\mu d\phi'}{\int_0^{2\pi}\int_0^1 \mu L^{(\downarrow}_{R+A}(\mu_s, \mu, \phi')\, d\mu d\phi'} \tag{16b}$$

$$\overline{\rho_s}'(\mu_s, \mu_v, \phi) = \overline{\rho_s}(\mu_v, \mu_s, \phi) \tag{16c}$$

$$\overline{\overline{\rho_s}}(\mu_s, \mu_v, \phi) = \overline{\overline{\rho_s}'}(\mu_v, \mu_s, \phi) \tag{16d}$$

Where $L^{\downarrow}_{R+A}(\mu_s, \mu, \phi')$ is the downwelling flux. Equation (16d) is approximated like the spherical albedo or white sky albedo, namely:

$$\overline{\overline{\rho_s}} \cong \int_0^1\int_0^1\int_0^{2\pi} \mu\rho_s(\mu, \mu', \phi' - \phi)d\mu d\mu' d\phi \tag{16e}$$

The BDRF of the target $\rho_s(\mu, \mu', \phi')$ is in general unknown for any geometrical condition for the purpose of atmospheric correction. However, we will assume that the BRDF shape can be determined a priori. This simplifying assumption is necessary since Equation (16a) shows that the Top of the Atmosphere reflectance is given in terms of integrals of the BRDF of the surface Equations (16b-e). In other words, Equation (16a) is a non-linear integral equation for the BRDF function. Solving this equation rigorously in an operational setting is prohibitive since it would require multiple iterations of a radiative transfer model.

The unknown reflectance is the line-of-sight reflectance $\rho_s(\mu_s, \mu_v, \phi)$ but the BRDF of the target $\rho_s(\mu, \mu', \phi')$ is assumed to satisfy:

$$\rho_s(\mu,\mu',\phi') = \rho_s(\mu_s,\mu_v,\phi)\frac{\rho_m(\mu,\mu',\phi')}{\rho_m(\mu_s,\mu_v,\phi)} \tag{17a}$$

Where $\rho_s(\mu,\mu',\phi')$ is the "modeled" BRDF and the ratio $\frac{\rho_m(\mu,\mu',\phi')}{\rho_m(\mu_s,\mu_v,\phi)}$ is the BDRF shape. Using this assumption, Equation (16b) can be rewritten as:

$$\bar{\rho_s}(\mu_s,\mu_v,\phi) = \frac{\rho_s(\mu_s,\mu_v,\phi)}{\rho_m(\mu_s,\mu_v,\phi)}\rho_m(\mu_s,\mu_v,\phi) = \rho_s(\mu_s,\mu_v,\phi)\overline{\rho_m}^{shape}(\mu_s,\mu_v,\phi) \tag{17b}$$

And similarly for Equations (16c) and (16e):

$$\bar{\rho_s}'(\mu_s,\mu_v,\phi) = \frac{\rho_s(\mu_s,\mu_v,\phi)}{\rho_m(\mu_s,\mu_v,\phi)}\rho_m(\mu_s,\mu_v,\phi) = \rho_s(\mu_s,\mu_v,\phi)\overline{\rho_m}'^{shape}(\mu_s,\mu_v,\phi) \tag{17c}$$

$$\begin{aligned}\bar{\bar{\rho}}_s(\mu_s,\mu_v,\phi) &\cong \frac{\rho_s(\mu_s,\mu_v,\phi)}{\rho_m(\mu_s,\mu_v,\phi)}\int_0^1\int_0^1\int_0^{2\pi}\mu\rho_m(\mu_s,\mu_v,\phi)d\mu d\mu' d\phi \\ &= \rho_s(\mu_s,\mu_v,\phi)\overline{\rho_m}'^{shape}(\mu_s,\mu_v,\phi)\end{aligned} \tag{17d}$$

So, Equation (16a) is written as:

$$\begin{aligned}\rho_{TOA}(\mu_s,\mu_v,\phi) &= \rho_{R+Aer}(\mu_s,\mu_v,\phi) \\ &+ \rho_s(\mu_s,\mu_v,\phi)\left[e^{-\frac{\tau}{\mu_s}}e^{-\frac{\tau}{\mu_v}} + e^{-\frac{\tau}{\mu_s}}t_d(\mu_v)\overline{\rho_m}^{shape}\right. \\ &\left. + e^{-\frac{\tau}{\mu_s}}t_d(\mu_v)\overline{\rho_m}'^{shape} + t_d(\mu_v)t_d(\mu_s)\overline{\bar{\rho}_m^{shape}}\right] \\ &+ \rho_s(\mu_s,\mu_v,\phi)^2\frac{T_{R+Aer}\mu_s T_{R+Aer}S_{R+Aer}\left(\overline{\bar{\rho}_m^{shape}}\right)^2}{1 - S_{R+Aer}\overline{\bar{\rho}_m^{shape}}}\end{aligned} \tag{18}$$

Equation (18) is a quadratic equation in $\rho_s(\mu,\mu',\phi')$ that has only one positive solution since the product of the roots is negative. Therefore, solving for $\rho_s(\mu,\mu',\phi')$ is straightforward once each other term of Equation (18) is computed. The computation of $\overline{\rho_m}^{shape}$, $\overline{\rho_m}'^{shape}$ and $\overline{\bar{\rho}_m^{shape}}$, which are the only quantities not fully defined in the previous section, is described in the operational approach (next).

The model of BRDF used for $\rho_m(\mu_s,\mu_v,\phi)$ is the LiSparse-Reciprocal (LSR), RossThick (RT) linear kernel model, also used in the operational algorithm for the MODIS Albedo/BRDF product, that is written as:

$$\rho_m(\mu_s,\mu_v,\phi) = P_1 + P_2K_{LSR}(\mu_s,\mu_v,\phi) + P_3K_{RT}(\mu_s,\mu_v,\phi) \tag{19}$$

Where:

$$K_{RT}(\mu_s,\mu_v,\phi)=\frac{\left(\frac{\pi}{2}-\xi\right)cos\xi+sin\xi}{\mu_s+\mu_v}-\frac{\pi}{4}$$

$$cos\xi=\mu_s\mu_v+\sqrt{1-\mu_s}\sqrt{1-\mu_v}cos\phi$$

$$K_{LSR}(\mu_s,\mu_v,\phi)=O(\mu_s,\mu_v,\phi)-\frac{1}{\mu_s}-\frac{1}{\mu_s}+\frac{1}{2}(1+cos\xi)\frac{1}{\mu_s}\frac{1}{\mu_v}$$

$$O(\mu_s,\mu_v,\phi)=\frac{1}{\pi}(t-\sin t\cos t)(\frac{1}{\mu_s}+\frac{1}{\mu_v})$$

$$cost=\frac{h}{b}\frac{\sqrt{D^2+tan\theta'}}{sec\theta'+sec\vartheta'}$$

$$D^2=\sqrt{\tan^2\theta'+\tan^2\vartheta'-2\tan\theta'\tan\vartheta'\,cos\phi}$$

$$\theta'=\tan^{-1}\frac{b}{r}\tan\theta_s \qquad \vartheta'=\tan^{-1}\frac{b}{r}\tan\theta_v$$

where, h describes the crown model central height above the ground, and r and b describe the vertical and horizontal dimensions of the crown spheroid, respectively. The interesting properties of this BRDF model are that the geometrical conditions are decoupled from the surface weighting parameters, therefore:

$$\overline{\rho_m}^{shape}(\mu_s,\mu_v,\phi)=\frac{1+\frac{P_2}{P_1}\overline{K_{LSR}}(\mu_s,\mu_v,\phi)+\frac{P_3}{P_1}\overline{K_{RT}}(\mu_s,\mu_v,\phi)}{1+\frac{P_2}{P_1}K_{LSR}(\mu_s,\mu_v,\phi)+\frac{P_3}{P_1}K_{RT}(\mu_s,\mu_v,\phi)} \tag{20}$$

By pre-computing the downward irradiance integrals $\overline{K_{LSR}}(\mu_s,\mu_v,\phi)$ and $\overline{K_{RT}}(\mu_s,\mu_v,\phi)$ for the kernels $K_{LSR}(\mu_s,\mu_v,\phi)$ and $K_{RT}(\mu_s,\mu_v,\phi)$ and storing them in lookup tables (they are a function of the band i, the optical thickness at 550nm, and the aerosol model), the functions $\overline{\rho_m}^{shape}(\mu_s,\mu_v,\phi)$ and their associated ($\overline{\rho_m}'^{shape}$ and $\overline{\overline{\rho_m^{shape}}}$) can be recomputed on the fly. The only unknown at this point is the weight of the BRDF shape function, $P_2'=\frac{P_2}{P_1}$ and $P_3'=\frac{P_3}{P_1}$.

Some experiments with MODIS data have shown that the BRDF shape parameter can be fitted as a function of NDVI. That is, to a first order, for low NDVI, low vegetation cover, P_2' and P_3' are expected to be near zero since the BDRF effects are small, while for higher NDVI, the coefficients are expected to be higher. It should be noted that P_2' and P_3' depend on the band as well. In the present version of the code, a linear interpolation is performed between a semi-arid case (low NDVI) and a forest case (high NDVI) for which the P_2' and P_3' have been

inverted using as large a data record as possible. More details can be found in Vermote et al., 2009.

3.4.1.4 Thin cirrus correction

Should thin cirrus (presently defined to possess optical thickness at 640 nm ranging up to 1) be present, the Surface Reflectance and downstream products are generated but with associated flags indicated in the "QA" variable. The baseline approach for removing much of the thin cirrus-laden pixels is very simple. It assumes that cirrus reflectance is not spectrally dependent, and that cirrus reflectance is spatially homogeneous. This allows the application of a threshold adjustment to all VIIRS bands in the general form:

$$\rho_\lambda = \rho_\lambda - \left(\frac{\rho_{1.38}}{T_{H_2O}^{1.38}}\right) \tag{21}$$

Where ρ_λ is the reflectance at the particular band, $\rho_{1.38}$ is the reflectance at the 1.38-micron VIIRS band, and $T_{H_2O}^{1.38}$ is the total two-way transmittance of water vapor at 1.38 microns for the given solar and viewing geometry. $T_{H_2O}^{1.38}$ is assumed to be 0.6, based on Vermote and Vermeulen (1999).

This correction is applied to the radiances in the other VIIRS reflective bands prior to the application of the Lambertian correction. The inherent assumption within Equation (21), even at VIIRS scale, may not be valid under every circumstance, but suspected pixels are nonetheless flagged. A few reasons why the assumption might not be valid include: cirrus ice crystals are not spatially homogeneous and there may be cirrus adjacency issues. Vermote and Vermeulen (1999) provides additional insights.

3.4.1.5 BRDF correction

The analysis of Parasol multidirectional data has shown that, among analytical BRDF models, the Ross–Li–Maignan model provides the best fit to the measurements (Breon et al. 2002). This model computes the reflectance as the sum of three terms:

$$\rho(\theta_v, \theta_s, \phi, \lambda) = k_{iso}(\lambda) + k_{geo}(\lambda)F_{geo}(\theta_v, \theta_s, \phi) + k_{vol}(\lambda)F_{vol}(\theta_s, \theta_v, \phi) \tag{22}$$

Which can be written as:

$$\rho(\theta_v, \theta_s, \phi, t) = k_{iso}(t)[1 + \boldsymbol{R}F_{geo}(\theta_v, \theta_s, \phi) + \boldsymbol{V}F_{vol}(\theta_v, \theta_s, \phi)] \tag{23}$$

where F_{vol} is the volume scattering kernel, based on the Ross-thick function, but corrected for the Hot-Spot process, and F_{geo} is the geometric kernel, based on the Li-sparse reciprocal function. $F_{vol}$and F_{geo} are fixed functions of the observation geometry, but k_{geo}, k_{vol}, and k_{iso} are free parameters. To simplify notation, V = k_{vol}/k_{iso} and R = k_{geo}/k_{iso}. The F_{vol} and F_{geo} functions are given in (24) and (25).

$$F_{geo}(\theta_s, \theta_v, \phi) = \frac{m}{\pi}(t - \sin t - \cos t - \pi) + \frac{1 + \cos\xi}{2\cos\theta_s \cos\theta_v} \tag{24}$$

$$\cos t = \frac{2}{\sec\theta_s + \sec\theta_v}\sqrt{\Delta^2 + (\tan\theta_s \tan\theta_v \sin\phi)^2}$$

$$\Delta^2 = \tan^2\theta_s + \tan^2\theta_v - 2\tan\theta_s \tan\theta_v \cos\phi$$

$$m = \frac{1}{cos\theta_s} + \frac{1}{\cos\theta_v}$$

$$cos\xi = cos\theta_s * \cos\theta_v + sin\theta_s sin\theta_v cos\phi$$

$$F_{vol}(\theta_s, \theta_v, \phi) = \frac{4}{3\pi}\frac{1}{cos\theta_s + cos\theta_v}\left[\left(\frac{\pi}{2} - \xi\right)\cos\xi + sin\xi\right]\left(1 + \left(1 + \frac{\xi}{\xi_0}\right)^{-1}\right) - \frac{1}{3} \quad (25)$$

where ξ is the scattering angle and ξ_0 is a characteristic angle that can be related to the ratio of scattering element size and the canopy vertical density (ξ_0 =1.5°).

A correction of the directional effect is derived after transforming the measurement coordinates to standard observation geometry. In the following, the standard observation geometry is for the Sun at 45° from zenith, and the observation at nadir. The normalized reflectance is therefore computed as

$$\rho^N(45,0,0) = \rho(\theta_s, \theta_v, \phi) * \frac{1 + VF_{\text{vol}}(45,0,0) + RF_{\text{geo}}(45,0,0)}{1 + VF_{vol}(\theta_s, \theta_v, \phi) + RF_{\text{geo}}(\theta_s, \theta_v, \phi)} \quad (26)$$

BRDF correction is based on pre-computed coefficients (V_0, V_1, R_0, R_1) describing the relationship of V and R with NDVI (Vermote et al. 2009).

$$V = V_0 + V_1 * NDVI$$
$$R = R_0 + R_1 * NDVI \quad (27)$$

The 4 coefficients (V_0, V_1, R_0, R_1) were retrieved using the 2000-2011 MODIS archives following the approach presented in Vermote et al. 2009. These coefficients serve as the LUTs. Figure 3 illustrates global maps of V and R derived from MODIS 2000-2004.

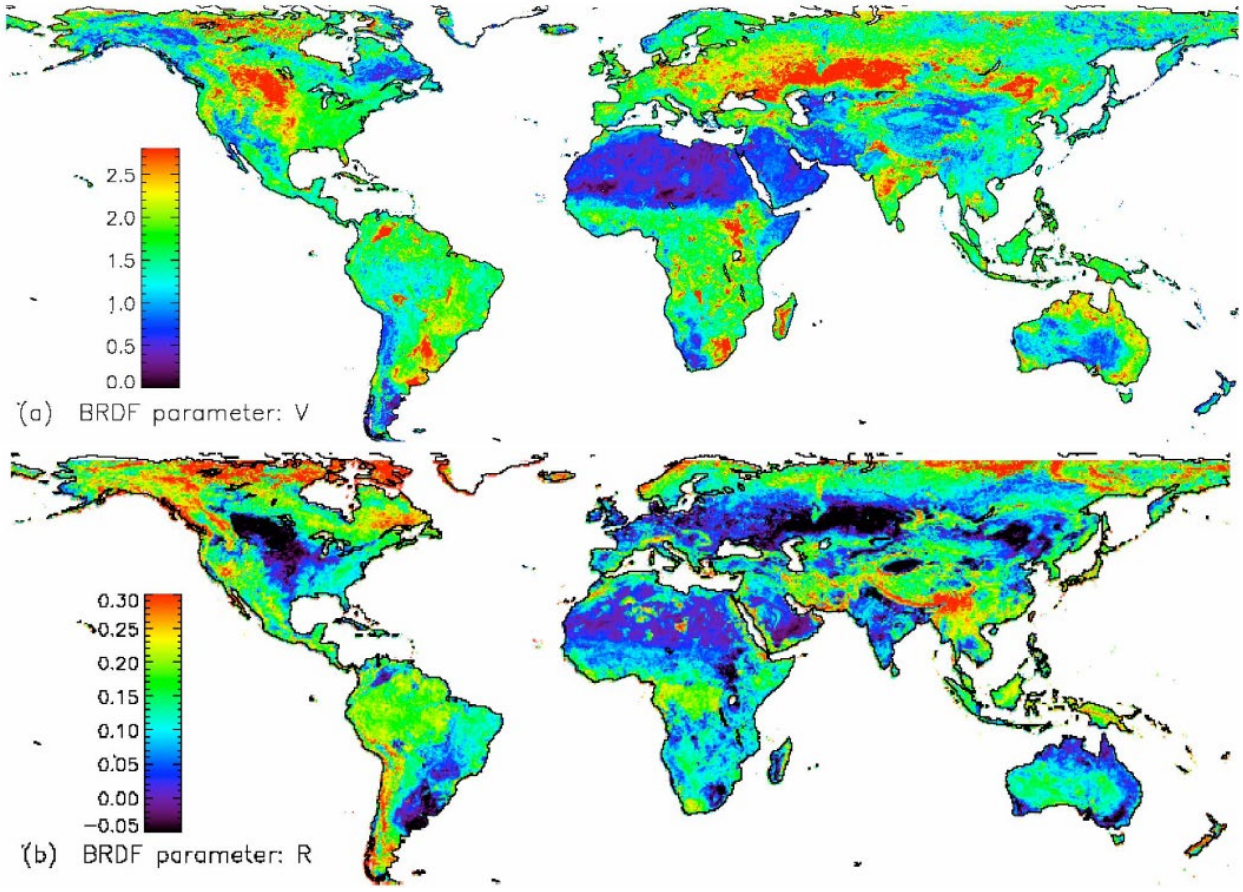

Figure 3: Global map of the V (a) and R (b) parameters derived by Vermote et al. 2009 applied to the time series of Terra MODIS band 2 (2000–2004). V and R are shown for highest NDVI values of each pixel.

3.4.1.6 NDVI Computation

NDVI is computed using bands I1 and I2:

$$NDVI = \frac{\rho_{NIR} - \rho_{red}}{\rho_{NIR} + \rho_{red}} = \frac{I_2 - I_1}{I_2 + I_1} \quad (27)$$

3.4.2 Data Merging Strategy

N/A

3.4.3 Numerical Strategy

N/A

3.4.4 Calculations

N/A

3.4.5 Look-Up Table Description

The BRDF look-up table is described in section 3.4.1.5. For the atmospheric look-up tables, the quantities $\rho_0(\mu_s, \mu_v, \phi)$, $td(\mu)$, and S are functions of the optical thickness (τ), single scattering albedo (ω), and phase function (P(θ)) of the scatterers and absorbers in the atmosphere. The calculation of $\rho_0(\mu_s, \mu_v, \phi)$, $td(\mu)$, and S is achieved with the aid of an atmospheric radiative transfer program such as the Dave and Gazdag (1970) model. However, it is computationally prohibitive to run a radiative transfer model for every pixel in a daily global data set. Thus, we created look-up tables with the 6S code (Vermote et al., 1997) which will supply the needed $\rho_0(\mu_s, \mu_v, \phi)$, $td(\mu)$, and S for a variety of sun-view geometries and aerosol loadings. $\rho_0(\mu_s, \mu_v, \phi)$ are precomputed at 73 relative azimuth angles, 22 solar zenith angles, 22 view zenith angles and 10 aerosol optical depth. $td(\mu)$, is precomputed for 16 zenith angles and 10 aerosol optical thickness. S is precomputed for 10 aerosol optical thickness.

3.4.6 Parameterization

N/A

3.4.7 Algorithm Output

The outputs products are 2 NetCDF files per day as detailed in Table 1. Tables 5 and 6 show details of the layers of each product. An example filename is:

VIIRS-Land_v001-preliminary_NPP09C1_SNPP_20210424_c20210505165924.nc

With the following naming convention:

<product-name> = static series name of the product with the value, “VIIRS-Land”

<***product-version***> = product version number, “v001”

<***product-type***> = NOAA product type identifier with the valid domain:

“NPP09C1” = VIIRS surface reflectance product from SNPP

“NPP13C1” = VIIRS NDVI product from SNPP

“JP109C1” = VIIRS surface reflectance product from JPSS-1

“JP113C1” = VIIRS NDVI product from JPSS-1

<satellite> = satellite: “SNPP”, “NOAA-20”, etc

<***YYYYmmdd***> = Date of the data in the file, formatted as year, month and day

c<***processing-date***> = Creation or processing date of the file identified with a ‘c’ followed by the year, month, day, hour, minute and second

.nc indicates the format (NetCDF)

Table 5: Layers of the NPP09C1/JP109C1 product

Variable name	Description	Dimensions	Data Type
'latitude'	Latitude of the pixel's center	3600 × 1	single
'longitude'	Longitude of the pixel's center	7200 × 1	single
'time'	Time of acquisition ('days since 1981-01-01 00:00:00')	1	single
'crs'	Coordinate reference system	1	Int16
'lat_bnds'	Latitude of pixel's edges	3600 × 2	single
'lon_bnds'	Longitude of pixel's edges	7200 × 2	single
'BRDF_corrected_I1_SurfRefl_CMG'	I1 band BRDF corrected surface reflectance	3600 × 7200	Int16
'BRDF_corrected_I2_SurfRefl_CMG'	I2 band BRDF corrected surface reflectance	3600 × 7200	Int16
'BRDF_corrected_I3_SurfRefl_CMG'	I3 band BRDF corrected surface reflectance	3600 × 7200	Int16
'BT_CH12'	M12 band Brightness Temperature	3600 × 7200	Int16
'BT_CH15'	M15 band Brightness Temperature	3600 × 7200	Int16
'BT_CH16'	M16 band Brightness Temperature	3600 × 7200	Int16
'SZEN'	Solar Zenith Angle	3600 × 7200	Int16
'VZEN'	View Zenith Angle	3600 × 7200	Int16
'RELAZ'	Relative Azimuth Angle	3600 × 7200	Int16
'TIMEOFDAY'	Time (hours) since 00:00:00	3600 × 7200	Int16
'QA'	Quality Control	3600 × 7200	Int16

Table 6: Layers of the NPP13C1/JP113C1 product

Variable name	Description	Dimensions	Data Type
‘latitude’	Latitude of the pixel’s center	3600 × 1	single
‘longitude’	Longitude of the pixel’s center	7200 × 1	single
‘time’	Time of acquisition ('days since 1981-01-01 00:00:00')	1	single
‘crs’	Coordinate reference system	1	Int16
‘lat_bnds’	Latitude of pixel’s edges	3600 × 2	single
‘lon_bnds’	Longitude of pixel’s edges	7200 × 2	single
‘NDVI’	Normalized Difference Vegetation Index	3600 × 7200	Int16
'SZEN'	Solar Zenith Angle	3600 × 7200	Int16
'VZEN'	View Zenith Angle	3600 × 7200	Int16
'RELAZ'	Relative Azimuth Angle	3600 × 7200	Int16
'TIMEOFDAY'	Time (hours) since 00:00:00	3600 × 7200	Int16
'QA'	Quality Control	3600 × 7200	Int16

Test Datasets and Outputs

3.5 Test Input Datasets

N/A

3.6 Test Output Analysis

3.6.1 Reproducibility

N/A

3.6.2 Precision and Accuracy

N/A

3.6.3 Error Budget

The Surface Reflectance algorithm performance may be affected by sensor, solar and viewing geometry effects including target elevation above sea level, atmospheric, and coupling of the atmosphere and surface effects, i.e., BRDF, among others. The atmospheric effects include aerosol and Rayleigh scattering, gaseous absorption, and thermodynamic conditions. The largest atmospheric effects on surface reflectance retrieval are from variations in aerosol properties. Sensor calibration is the primary contributor to sensor effects.

There are no explicit quality requirements on the Surface Reflectance in the VIIRS SRD. We have, however, derived performance requirements for surface reflectance retrievals to assist in the interpretation of our algorithm sensitivity tests. The requirements for surface reflectance are primarily derived from the specification requirements placed on the Vegetation Index Environmental Data Record (EDR), and the Surface Albedo EDR. The Surface Albedo EDR requires that the surface reflectance values be retrieved to within 0.05 of an albedo unit. For example, Liang et al. (2002) showed that when the surface reflectance values (derived from MODIS products) were within 5% absolute error, the resulting broadband albedo values had an absolute error within 2%. The Vegetation Index EDR has two general components, the Normalized Difference Vegetation Index (NDVI) and the Enhanced Vegetation Index (EVI). The implied specification on the top of canopy (TOC) EVI requires that in the most stringent case the VIIRS surface reflectance values be retrieved to within 0.012 of a surface reflectance unit. This would be sufficient to meet the specification on EVI, but it is not necessary.

The absolute error in the retrieved surface reflectance assuming a Lambertian surface is typically 0.02 to 0.06 of a unit for a clear atmosphere to 0.03-0.11 for a hazy atmosphere (aerosol optical thickness of 0.5) at a solar zenith angle of 60 degrees and at the maximum backscattering point (i.e., at the hot spot). Thus, to meet the system specification, set for the vegetation index as well as the surface albedo, further adjustments are likely to be necessary.

The current lack of sufficient data and final spectral response functions for VIIRS mandates that we perform a preliminary verification investigation of the VIIRS output against the corresponding output from MODIS despite their spectral and spatial differences. The result of this investigation requires a close agreement with the MODIS heritage sensor data, particularly in the VIIRS M4 and MODIS band 4 spectral region, where the spectral differences between the two sensors are minimal, for this algorithm to have a chance of meeting the derived requirements.

4. Practical Considerations

4.1 Numerical Computation Considerations

N/A

4.2 Programming and Procedural Considerations

N/A

4.3 Quality Assessment and Diagnostics

The estimate of the surface reflectance and NDVI is accompanied with quality assurance information. QA bits contain information stored at the product resolution. Details about the Quality Assessment and Quality Control layers for this product are shown in Table 6. Both surface reflectance and NDVI products have the same QA definitions. For example, users that seek to use the product for vegetation monitoring could use the flag combinations shown in bold in Table 6 to ensure the highest quality pixel.

Table 7: Quality control layer description.

Bit Number	Parameter Name	Bit Combination	Description
0-1	Cloud State	**00**	**Confident Clear**
		01	Probably Clear
		10	Probably Cloudy
		11	Confident Cloudy
2	Cloud shadow	1	Yes
		0	**No**
3-5	Land/Water flag	**000**	**Land & Desert**
		001	Land no desert
		010	Inland Water
		011	Sea Water
		100	---
		101	Coastal
		110	---
		111	---
6	Overall Aerosol Quality	**1**	**OK**
		0	Poor
7	Unused	---	---
8	Thin cirrus reflective	1	Yes
		0	**No**

9	Thin cirrus emissive	1	Yes
		0	**No**
10	Cloud flag	1	Cloud
		0	**No cloud**
11-14	Unused	---	---
15	Snow/Ice Flag	1	Snow/Ice
		0	**No snow/Ice**

4.4 Exception Handling

N/A

4.5 Algorithm Validation

N/A

4.6 Processing Environment and Resources

The CDR code is run on an 8-core 2.5GHz 64-bit Xeon server, running CentOS Linux 3.10 x86_64. The code was compiled with C-compiler GCC 4.8.5. The main C-libraries were: HDF5 1.8.12, HDF 4.2r10, NetCDF 4.2, Zlib 1.2, szip. A full year of NPP09C1 and NPP13C1 products is processed in 3.5 days corresponding approximately to a 100x speed.

5. Assumptions and Limitations

5.1 Algorithm Performance

This algorithm is constrained to land areas even if non-land areas are provided. Extreme angles may cause large errors.

5.2 Sensor Performance

<Not Applicable>

6. Future Enhancements

N/A

7. References

Bréon, Francois-Marie, et al. "Analysis of hot spot directional signatures measured from space." Journal of Geophysical Research: Atmospheres 107.D16 (2002): AAC-1.

Dave, Jitendra V., and J. Gazdag. "A modified Fourier transform method for multiple scattering calculations in a plane parallel Mie atmosphere." Applied Optics 9.6 (1970): 1457-1466.

Deschamps P.Y., Herman M., Tanre D, 1983, Modeling of the atmospheric effects and its application to the remote sensing of Ocean Color, Applied Optics , 22 (23): 3751-3758.

Liang, S., others (2002). Validating MODIS land surface reflectance and albedo products: methods and preliminary results. Remote Sensing of Environment, 83 001-014.

Putsay, M. "A simple atmospheric correction method for the short wave satellite images." International Journal of Remote Sensing 13.8 (1992): 1549-1558.

Vermote, E.F., and A. Vermeulen (1999). Atmospheric correction algorithm: spectral reflectances (MOD09). Version 4.0. Algorithm technical background document. NASA EOS-1D 2015 Doc.

Vermote, E.F., D. Tanré, J.L. Deuzé, M. Herman, and J.J. Morrisette (1994). Second Simulation of the Satellite Signal in the Solar Spectrum (6S), 6S Version 0 User's Guide, April 18. NASA Goddard Space Flight Center, 183 pp.

Vermote, E.F., D. Tanré, J.L. Deuzé, M. Herman, and J.J. Morrisette (1997). Second Simulation of the Satellite Signal in the Solar Spectrum, 6S: An Overview. IEEE Transactions on Geoscience and Remote Sensing, 35, 675-686.

Vermote, E., Justice, C. O., & Bréon, F. M. (2009). Towards a generalized approach for correction of the BRDF effect in MODIS directional reflectances. IEEE Transactions on Geoscience and Remote Sensing, 47(3), 898–908. http://doi.org/10.1109/TGRS.2008.2005977

Appendix A. Acronyms and Abbreviations

Acronym or Abbreviation	Meaning
6S	Second Simulation of a Satellite Signal in the Solar Spectrum
AERONET	AErosol RObotic NETwork
AOT	Aerosol Optical Thickness
AVHRR	Advanced Very High Resolution Radiometer
BRDF	Bidirectional reflectance distribution function
C-ATBD	Climate Algorithm Theoretical Basis Document
CDR	Climate Data Record
DEM	Digital elevation model
EDR	Environmental Data Record
GAC	Global Area Coverage
LSB	Least significant bit
LTDR	Long Term Data Record
MODIS	Moderate Resolution Imaging Spectroradiometer
MSB	Most Significant Bit
NCEP	National Centers for Environmental Prediction
NDVI	Normalized Difference Vegetation Index
NIR	Near infrared
NOAA	National Oceanic and Atmospheric Administration
PAL	Pathfinder Land
QA	quality assurance
QC	quality control
SR	Surface Reflectance
TOA	top of atmosphere
TOC	top of canopy
VIIRS	Visible Infrared Imaging Radiometer Suite